STRUCTURAL BIOLOGY COMMUNICATIONS

ISSN 2053-230X

X-ray crystal structure of human calcium-bound S100A1

Zephan Melville,[a] Ehson Aligholizadeh,[a] Laura E. McKnight,[a] Dylan J. Weber,[a] Edwin Pozharski[a] and David J. Weber[a,b]*

[a]Center for Biomolecular Therapeutics, Department of Biochemistry and Molecular Biology, University of Maryland Baltimore, 108 North Greene Street, Baltimore, MD 21201, USA, and [b]Marlene and Stewart Greenebaum Cancer Center, University of Maryland Baltimore, 108 North Greene Street, Baltimore, MD 21201, USA. *Correspondence e-mail: dweber@som.umaryland.edu

Received 4 October 2016
Accepted 11 March 2017

Edited by R. J. Read, University of Cambridge, England

Keywords: S100; S100A1; crystal structure; calcium-binding proteins; S100B; Alzheimer's disease; cardiomyopathy.

PDB reference: S100A1, 5k89

Supporting information: this article has supporting information at journals.iucr.org/f

S100A1 is a member of the S100 family of Ca^{2+}-binding proteins and regulates several cellular processes, including those involved in Ca^{2+} signaling and cardiac and skeletal muscle function. In Alzheimer's disease, brain S100A1 is overexpressed and gives rise to disease pathologies, making it a potential therapeutic target. The 2.25 Å resolution crystal structure of Ca^{2+}-S100A1 is solved here and is compared with the structures of other S100 proteins, most notably S100B, which is a highly homologous S100-family member that is implicated in the progression of malignant melanoma. The observed structural differences in S100A1 *versus* S100B provide insights regarding target protein-binding specificity and for targeting these two S100 proteins in human diseases using structure-based drug-design approaches.

1. Introduction

S100 proteins are a family of Ca^{2+}-binding proteins with cell-specific and tissue-specific expression and a variety of intracellular and extracellular regulatory functions (Baudier *et al.*, 1986; Donato *et al.*, 2013; Donato, 2001; Zimmer *et al.*, 1995). Despite having no enzymatic activity, S100 proteins are involved in a range of biological processes, including Ca^{2+} homeostasis, cell growth, metabolism and phosphorylation (Donato *et al.*, 2013; Kligman & Hilt, 1988; Schäfer & Heizmann, 1996; Strynadka & James, 1989; Zimmer *et al.*, 1995). The influence of S100 proteins is typically mediated through Ca^{2+}-dependent protein–protein interactions (PPIs). With calbindin as the exception, S100 proteins assemble as homodimers or heterodimers, with each subunit having two EF-hand domains termed EF1 and EF2. The N-terminal EF-hand, EF1, is a pseudo EF-hand having 14 amino-acid residues (*versus* 12) and binds calcium with a lower affinity than EF2. The canonical EF-hand, EF2, resides in the C-terminal region of an S100 subunit and Ca^{2+}-binding to EF2 activates the rotation of helix 3 necessary for target protein binding (Wright, Inman *et al.*, 2008; Wright *et al.*, 2009). The altered expression of several S100 proteins is associated with a variety of disease states, including cancer (Bresnick *et al.*, 2015; Harpio & Einarsson, 2004; Rustandi *et al.*, 1998; Salama *et al.*, 2008), neurological disorders (Bresnick *et al.*, 2015; Most *et al.*, 2007; Salama *et al.*, 2008) and cardiomyopathies (Bresnick *et al.*, 2015; Most *et al.*, 2007; Salama *et al.*, 2008), with several S100 proteins (*i.e.* S100A1, S100A4, S100A7, S100B and others) being considered as potential therapeutic targets for drug development (Bresnick *et al.*, 2015; Harpio & Einarsson, 2004; Malashkevich *et al.*, 2008; Salama *et al.*, 2008).

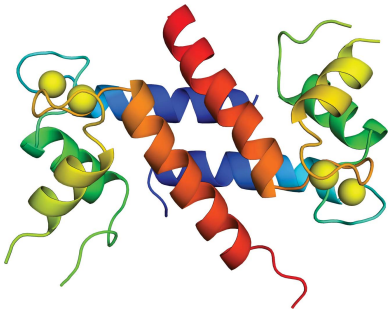

Table 1
Crystallographic statistics.

Values in parentheses are for the highest resolution shell.

Diffraction source	Beamline 7-1, SSRL
Wavelength (Å)	1.1271
Resolution range (Å)	33.47–2.25 (2.33–2.25)
Space group	$P3_221$
a, b, c (Å)	53.5, 53.5, 193.4
α, β, γ (°)	90, 90, 120
Total No. of reflections	81192 (5079)
No. of unique reflections	15829 (765)
Mosaicity (°)	1.7
Multiplicity	5.1 (3.8)
Completeness (%)	92 (85)
$\langle I/\sigma(I)\rangle$	14.44 (0.39)
Overall B factor from Wilson plot (Å^2)	50.78
R_{merge}	0.185 (3.61)
R_{meas}	0.205 (4.17)
$CC_{1/2}$	0.99 (0.16)
CC*	1.00 (0.53)
No. of reflections, working set	16102 (764)
No. of reflections, test set	757 (38)
R_{work}	0.275 (0.491)
R_{free}	0.290 (0.528)
Cruickshank DPI	0.245
No. of non-H atoms	
Total	2093
Protein	2065
Ligand	14
Solvent	14
R.m.s. deviations	
Bonds (Å)	0.009
Angles (°)	0.96
Average B factors (Å^2)	
Overall	82.60
Protein	82.83
Ligand	73.56
Ramachandran plot	
Most favored (%)	96.0
Allowed (%)	4.0
PDB code	5k89

S100A1 is highly expressed in cardiac and skeletal muscle and interacts with a number of proteins, including the ryanodine receptor (RyR), an interaction that regulates Ca^{2+} transients in heart and skeletal muscle (Garbuglia *et al.*, 1999; Landar *et al.*, 1998; Most, Remppis, Pleger *et al.*, 2003; Most, Remppis, Weber *et al.*, 2003; Most *et al.*, 2004; Osterloh *et al.*, 1998; Treves *et al.*, 1997; Wang *et al.*, 2005; Wright *et al.*, 2009). In a heart-failure model, decreased S100A1 expression followed by adenoviral reintroduction of the S100A1 gene restored diminished Ca^{2+} transients and reversed contractile dysfunction (Most *et al.*, 2004). However, in the brain overexpressed S100A1 contributes to pathologies related to neurological diseases (Wright *et al.*, 2009). Specifically, high levels of extracellular S100A1 are cytotoxic and its intracellular processes augment Alzheimer's disease pathologies, including altered amyloid precursor protein expression, destabilization of calcium homeostasis, increased cell growth, decreased dendritic arborization and lower tubulin polymerization/stability (Wright *et al.*, 2009; Zimmer *et al.*, 1998). Thus, incentives to develop S100A1 antagonists are in place to regulate both its intracellular and extracellular functions when elevated in neurological diseases. On the other hand, blocking of S100A1 needs to be avoided when S100A1 levels are in the normal range so its critical roles in Ca^{2+}-signaling and muscle contraction remain functional. The approach of avoiding S100A1 blockade remains an important consideration for developing other S100 inhibitors, including S100B inhibitors for treating melanoma (Bresnick *et al.*, 2015). The crystal structure of Ca^{2+}-S100A1 is reported here to provide details for better understanding of S100-specific targets and for the development of S100A1-specific and/or S100B-specific inhibitors. Thus, the crystal structure of Ca^{2+}-S100A1 was determined and compared with previously published structures of S100A1 (NMR) and S100B (NMR, X-ray) to facilitate these goals as well as to better understand the structure–function relationships within the S100 protein family.

2. Methods

2.1. Materials

Chromatography columns and resins were obtained from GE Healthcare Life Sciences. All buffers were passed through Chelex-100 (Bio-Rad) to remove trace metals and divalent ions. All recombinant proteins were dialyzed using Chelex-100 resin for the same purpose. All other chemical reagents used were ACS grade or higher and were purchased from Sigma–Aldrich unless otherwise stated.

2.2. Expression and purification of S100A1

Recombinant human S100A1 was expressed in *Escherichia coli* strain BL21(DE3) cells transformed with an expression plasmid (pET-11b; Novagen) containing the gene for codon-optimized human S100A1. *E. coli* cultures were allowed to grow at 37°C to an OD_{600} of 0.8–1.0 and were induced with 1 m*M* isopropyl β-D-1-thiogalactopyranoside (IPTG) for 4 h or overnight (8 h) at 25°C. The cultures were then pelleted and stored at −80°C before purification. Lysis was performed at room temperature with buffer *A* (50 m*M* Tris–HCl pH 7.50, 0.5 m*M* DTT), 0.5 m*M* AEBSF, 1 mg lysozyme per gram of pellet, 0.5 mg DNAse I and 10 m*M* $MgCl_2$. Following this, sonication was performed on ice to ensure total cell lysis. The lysate was then pelleted and the supernatant was kept for precipitation with ammonium sulfate and streptomycin sulfate. Bacterial lysates were precipitated by the slow addition of ammonium sulfate to 65% saturation and streptomycin sulfate to 1%(*w*/*v*). The lysate was then pelleted again and the supernatant was dialyzed against buffer *A* to remove ammonium sulfate. The sample was loaded onto a DE52 diethylaminoethyl Sepharose (DEAE) column (Whatman). The column was equilibrated and unbound proteins were eluted with buffer *A*. S100A1 bound to the column was next eluted *via* stepwise additions of buffer with increasing NaCl concentrations. Fractions were analysed by SDS–PAGE, and S100A1 protein-containing fractions were pooled. Pure S100A1 (>99%) was concentrated (to >5 m*M*) and buffer-exchanged using gel filtration on a Sephadex G-25 column equilibrated in buffer *B* (0.25 m*M* Tris–HCl pH 7.50, 50 m*M* NaCl, 0.25 m*M* DTT). S100A1 from this column was concentrated (>5 m*M*) and stored frozen as separate aliquots to avoid repeated freeze–thaw cycles.

2.3. Crystallography

Diffraction-quality crystals of human S100A1 were obtained *via* sitting-drop vapor diffusion in 24-well trays (Hampton Research) using 250 µl reservoir solution and a 0.75:0.75 µl drop size. The mother liquor for crystal formation consisted of 100 m*M* cacodylate pH 7.0–7.5, 10 m*M* $CaCl_2$, 25–28% PEG 8000. The initial crystals were obtained under identical conditions using PEG 3350 in place of PEG 8000. The protein-sample conditions for crystal formation consisted of 20 mg ml^{-1} S100A1, 10 m*M* cacodylate pH 7.20, 7.5 m*M* $CaCl_2$; no cryoprotectants were used. Crystals were flash-cooled in liquid nitrogen for storage before data collection.

Remote data collection was performed on beamline 7-1 at the Stanford Synchrotron Radiation Lightsource (SSRL), SLAC National Accelerator Laboratory, Menlo Park, California, USA (Cohen *et al.*, 2002; Soltis *et al.*, 2008). Data were collected at 100 K on an ADSC Q315 (315 × 315 mm) detector using data-collection strategies generated by *Web-Ice* (González *et al.*, 2008). The diffraction statistics are summarized in Table 1. Processing of reflections was accomplished using the *AUTOXDS* script (González & Tsai, 2010) developed at SSRL to automate the existing *X-ray Detector Software* (*XDS*; Kabsch, 2010). The structure was initially solved in space group *C*2. Following this, however, we determined that the correct space group was in fact $P3_221$, as confirmed by *Zanuda* (Lebedev & Isupov, 2014), and the structure was solved again in this space group. The *BALBES* server (Long *et al.*, 2008) was utilized to identify an appropriate search model and to perform molecular replacement with *MOLREP* (Vagin, 1989; Vagin & Teplyakov, 1997, 2010). S100Z (PDB entry 2y5i) was identified as the best search model (Moroz *et al.*, 2011). Restrained refinement was performed using *phenix.refine* (Adams *et al.*, 2010; Afonine *et al.*, 2012) and *BUSTER-TNT* (Bricogne *et al.*, 2016), and manual building was performed in *Coot* (Emsley *et al.*, 2010). The structure-refinement statistics are summarized in Table 1, and final figures and alignments were made using *PyMOL* (http://www.pymol.org) unless otherwise stated.

3. Results and discussion

S100A1 is an enhancer of cardiac and skeletal muscle contractility and exhibits potential as a gene-therapeutic agent for the treatment of cardiomyopathies. S100A1 competes with calmodulin for binding RyR1 and acts as a sensitizer and activator of Ca^{2+} release (Prosser *et al.*, 2008, 2011; Schneider *et al.*, 2009; Wright, Prosser *et al.*, 2008; Yamaguchi *et al.*, 2011). On the other hand, when overexpressed in the brain, S100A1 contributes to pathologies related to neurological diseases (Wright *et al.*, 2009). Therefore, it is important to understand the specifics involved in the S100A1-dependent regulation of biological targets at atomic resolution. For this, the X-ray crystal structure of human Ca^{2+}-S100A1 is presented here, and comparisons of S100A1 and S100B are discussed in order to better understand the target-binding specificities required to generate unique biological responses.

3.1. X-ray crystal structure of calcium-bound S100A1

X-ray diffraction data were collected and the crystal structure of Ca^{2+}-bound S100A1 was solved at 2.25 Å resolution with R_{work} and R_{free} values of 0.275 and 0.290, respectively (Table 1; Fig. 1). The electron density was limited in places owing to anisotropy, particularly in loop regions such as the hinge region (loop 2) and the C-terminal loop. The asymmetric unit contains three S100A1 molecules: one full dimer and another monomer that forms the biological dimer by crystal symmetry. Like other members of the S100 protein family, S100A1 is a homodimer with an X-type four-helical bundle comprising its dimer interface (Fig. 1). Ca^{2+} coordination in the helix–loop–helix EF-hand domains of S100A1 could be modeled but not without some ambiguity owing to weaker electron density in these loops. For example, the

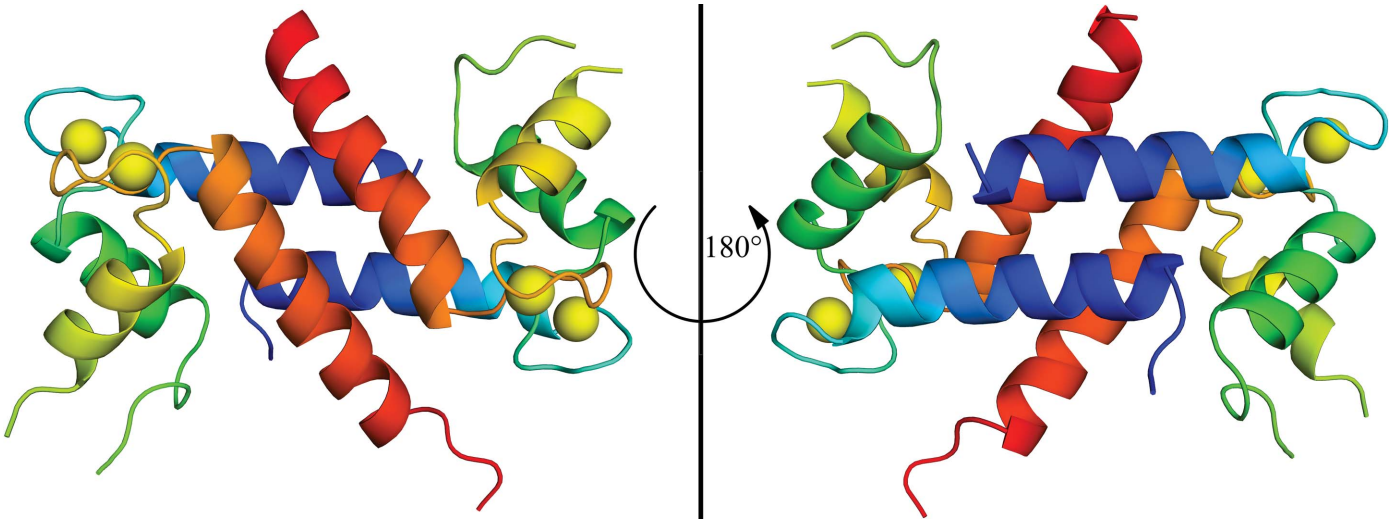

Figure 1
Ribbon diagram of the Ca^{2+}-S100A1 dimer crystal structure viewed from the front (left) and rear (right). Helices are colored blue, green, yellow and red for helices 1, 2, 3 and 4, respectively; Ca^{2+} ions are yellow.

Table 2
Intrahelical angles and distances for Ca^{2+}-S100A1 and other Ca^{2+}-S100 structures.

Intrahelical angles and distances were calculated using *UCSF Chimera* and previously established methods (Drohat *et al.*, 1998).

		Intrahelical angles (°)						Intrahelical distances (Å)					
	R.m.s.d. (Å)	I to II	I to III	I to IV	II to III	II to IV	III to IV	I to II	I to III	I to IV	II to III	II to IV	III to IV
S100A1 (X-ray)†	0.5	140.0	−116.5	127.4	103.4	−28.8	110.2	8.1	16.8	11.3	9.9	13.9	9.1
S100A1 (NMR)‡	2.6	133.3	−106.5	129.4	117.5	−33.0	119.7	9.8	19.5	13.4	10.2	12.4	8.5
S100A1–RyRP (NMR)§	2.5	137.8	−94.4	123.5	121.5	−40.6	137.2	9.7	19.3	12.4	10.4	12.6	9.9
S100A4 (X-ray)¶	1.5	140.2	−112.6	131.3	106.2	−34.9	108.5	8.1	17.2	11.1	10.0	13.6	8.8
S100B (X-ray)††	1.0	138.7	−126.6	126.7	93.8	−36.6	100.1	8.7	17.3	11.0	9.5	13.9	9.0
S100B (NMR)‡‡	2.9	131.9	−124.0	124.3	103.4	−38.7	103.1	10.4	20.1	12.1	10.2	13.2	9.9
S100Z (X-ray)§§	0.7	136.2	−107.6	131.8	116.2	−25.6	112.7	7.6	17.0	11.2	9.7	12.7	8.9

† The r.m.s.d. for the S100A1 crystal structure corresponds to the average alignment of each monomer in the asymmetric unit. ‡ Calculated using PDB entry 1zfs (Wright *et al.*, 2005). § Calculated using PDB entry 2k2f (Wright, Prosser *et al.*, 2008). ¶ Calculated using PDB entry 2q91 (Malashkevich *et al.*, 2008). †† Calculated using PDB entry 1mho (Matsumura *et al.*, 1998). ‡‡ Calculated using PDB entry 2k7o (Wright, Inman *et al.*, 2008). §§ Calculated using PDB entry 2y5i (Moroz *et al.*, 2011).

density for a water ligand at position 7 of each EF-hand was lacking, so it was not modeled for EF1 or EF2, as is typically found. Nonetheless, as in other S100 proteins, Ca^{2+} coordination in EF1 of S100A1 is *via* the O atoms of the backbone carbonyl moieties of Ser20, Glu23, Asp25, Lys28 and the side-chain carboxylate of Glu33, which coordinates in a bidentate manner. In EF2, Ca^{2+} coordination is *via* the side-chain carboxylate O atoms of Asp63, Asn65, Asp67, Glu74 and the

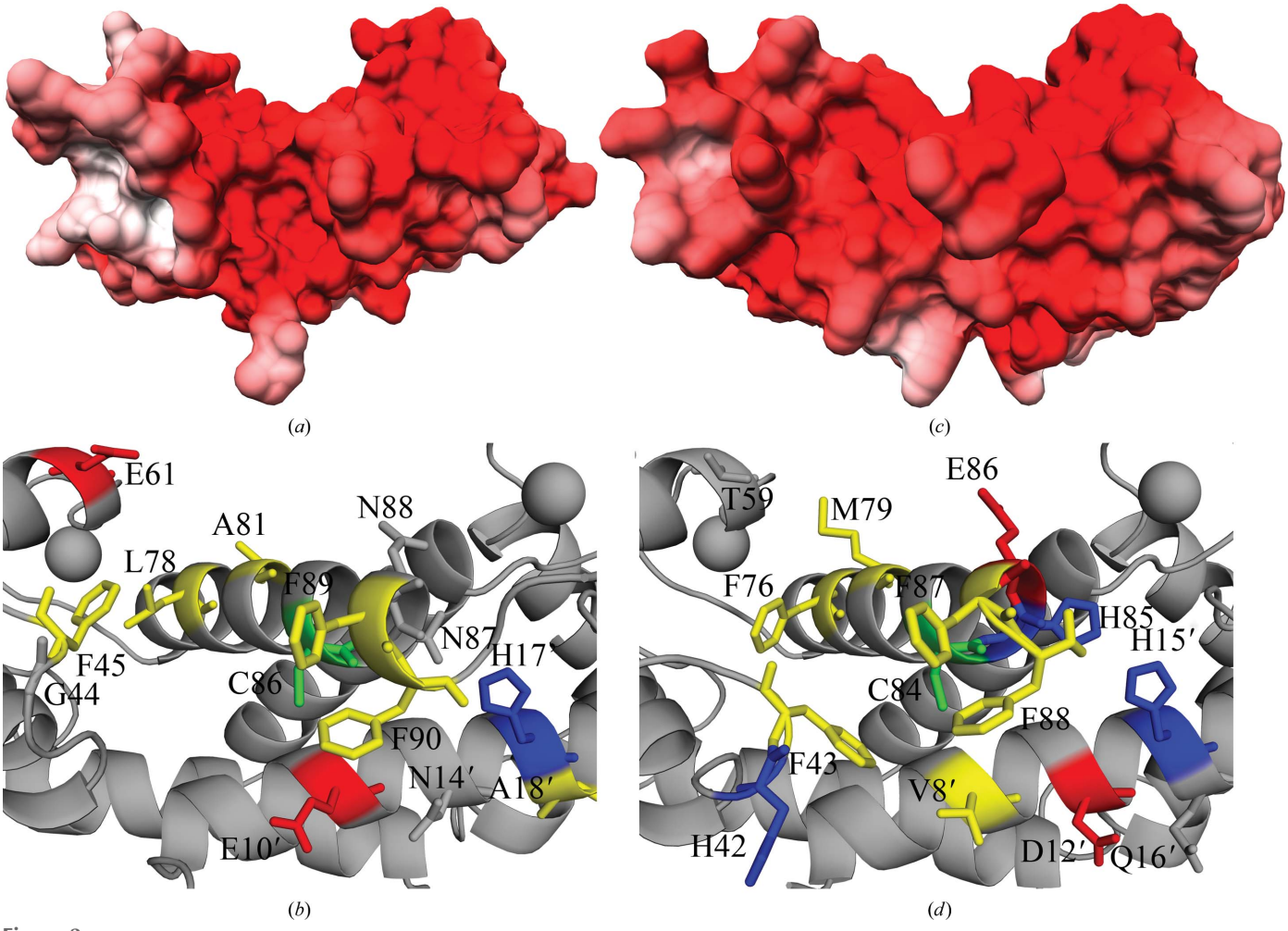

Figure 2
Left: electrostatic surface model (*a*) and ribbon diagram (*b*) of the Ca^{2+}-S100A1 crystal structure, highlighting the binding pocket. Right: electrostatic surface model (*c*) and ribbon diagram (*d*) of the Ca^{2+}-S100B crystal structure (PDB entry 1mho; Matsumura *et al.*, 1998). In the ribbon diagrams, hydrophobic residues are in yellow, positively charged residues are in blue and negatively charged residues are in red. Key residues are labeled; see text for additional details. Electrostatic surface models were generated using *PDB2PQR* (Dolinsky *et al.*, 2004, 2007), *APBS* (Czodrowski *et al.*, 2006) and *UCSF Chimera* (Pettersen *et al.*, 2004).

O atom of the backbone carbonyl moiety of Glu69, as is typical for canonical EF-hand motifs such as those in other S100 proteins, calmodulin, troponin C and other EF-hand-containing proteins (Strynadka & James, 1989). The one difference is that the O atom of Asn65 coordinates calcium in the EF2 domain of Ca^{2+}-S100A1 and this analogous coordination is *via* an O atom of an aspartate residue in S100B (Matsumura *et al.*, 1998).

The four helices in each subunit of Ca^{2+}-S100A1 and their alignment at the dimer interface of the crystal structure are very similar to that found previously *via* NMR (Table 2). This includes the perpendicular arrangement of helices 3 and 4 of Ca^{2+}-S100A1 to give an open conformation as is necessary to bind its protein targets, including a peptide derived from RyR1. In the absence of the RyR1 target peptide, the crystal and NMR structures of Ca^{2+}-S100A1 show a reasonable level of similarity when interhelical angles and metal-ion coordination distances are compared (Table 2). The crystal structure of Ca^{2+}-S100A1 aligns similarly with the NMR structures of Ca^{2+}-S100A1 in the absence (PDB entries 1zfs and 2lp3; Nowakowski *et al.*, 2013; Wright *et al.*, 2005) or presence (PDB entries 2k2f and 2kbm; Wright, Prosser *et al.*, 2008) of peptide targets (r.m.s.d. 2.3–2.6 Å) as well as other X-type helical bundle S100 proteins (Table 2). Differences in these and other S100 proteins are typically localized to the most dynamic regions of the proteins, including the hinge region (loop 2) and the C-terminus, which are involved in target binding.

3.2. Detailed comparison of S100A1 and S100B structures

When comparisons are made with S100B in particular, the global fold of Ca^{2+}-S100A1 determined here was also similar to those of several crystal structures available for S100B (Cavalier, Melville *et al.*, 2016; Drohat *et al.*, 1998; Gógl *et al.*, 2016; Jensen *et al.*, 2015). In such comparisons, the r.m.s.d. ranged between 0.7 and 1.2 Å, with the exception of S100B bound to a peptide derived from the receptor for advanced glycation endproducts (RAGE; PDB entry 5d7f, J. L. Jensen & C. L. Colbert, unpublished work; 1.6 Å r.m.s.d.), which diverges primarily in the dynamic C-terminus. When Ca^{2+}-coordination distances were compared for the S100A1 and S100B structures, they were also found to be essentially within the margin of error (all-atom alignment r.m.s.d. of 1.0 Å; Cruickshank DPI of the model of approximately 0.24 Å; *PyMOL*), so like other determined S100 protein structures, the crystal structure of Ca^{2+}-S100A1 determined here is similar in its overall global fold to other available S100 protein structures. In addition, similarities exist in the binding pockets of Ca^{2+}-S100A1 and Ca^{2+}-S100B. This includes the presence of a cysteine residue, Cys86 (Cys84 in S100B), bridging what are termed sites 1 and 2 of the target-binding pocket (Cavalier *et al.*, 2014; Charpentier *et al.*, 2009). While the target-binding pockets in Ca^{2+}-S100A1 and Ca^{2+}-S100B are composed largely of hydrophobic residues, it is clear that these pockets are not identical.

Upon closer comparison of Ca^{2+}-S100A1 and Ca^{2+}-S100B, there are structural differences that provide a means for specificity in target and inhibitor binding. Specifically, the binding pocket in Ca^{2+}-S100B has an additional aromatic residue (Phe76) available for π-stacking compared with an aliphatic residue (*i.e.* Leu78) in the analogous location in Ca^{2+}-S100A1 (Figs. 2 and 3). There is a negatively charged side chain on helix 3 (Glu61) in Ca^{2+}-S100A1 that is occupied by a polar residue (*i.e.* Thr59) in the analogous position in Ca^{2+}-S100B. In helix 4, a polar residue Asn87 in Ca^{2+}-S100A1 occupies a position where a positively charged His85 resides in Ca^{2+}-S100B. This histidine residue is also part of the Zn^{2+}-binding site in S100B (Wilder *et al.*, 2003), and S100A1 does not have this Zn^{2+}-binding site. In the hinge region (loop 2), the positively charged His42 in Ca^{2+}-S100B differs from the Gly44 in Ca^{2+}-S100A1. In the hinge region, the positions of Glu45, Glu46 and Ile47 in Ca^{2+}-S100B are occupied by Asp47, Ala48 and Gln49 in Ca^{2+}-S100A1 (Fig. 3). Another difference can be observed for Glu10, Asn14 and Ala18 in the target-binding pocket of Ca^{2+}-S100A1 *versus* Val8, Asp12 and Gln16 in the analogous positions of Ca^{2+}-S100B, which again would alter the mode of target and inhibitor binding. Thus, there are important differences in charge and polarity when the two binding pockets of these S100s are compared. These would additionally contribute to the specificity upon target binding and functional folding events necessary for Ca^{2+}-binding affinities to increase, as have been observed previously for S100B (Charpentier *et al.*, 2010; Liriano *et al.*, 2012; Rustandi *et al.*, 1998; Zimmer & Weber, 2010). With these observed differences, there are numerous structural and dynamic properties within Ca^{2+}-S100A1 and Ca^{2+}-S100B that can be used to explain mechanistically how these two proteins bind specific protein targets in a cell-specific manner to generate unique biological responses, as has been observed in many biological studies (Bresnick *et al.*, 2015; Donato *et al.*, 2013;

Figure 3
Sequence alignments.. Sequence alignments were generated using *T-Coffee* (Di Tommaso *et al.*, 2011; Notredame *et al.*, 2000) and *BoxShade*. S100A sequences correspond to the human sequence, S100B corresponds to the bovine sequence and S100Z corresponds to the zebrafish sequence.

Hernández-Ochoa *et al.*, 2009; Lin *et al.*, 2010; Wright, Prosser *et al.*, 2008; Wright *et al.*, 2009; Zimmer *et al.*, 1995; Zimmer & Weber, 2010).

4. Conclusions

The crystal structure of Ca^{2+}-S100A1 is presented here at 2.25 Å resolution. As a complement to the previously published NMR data, crystallography provides a detailed examination of the atomic structure of S100A1 and its binding pocket to reveal small but significant differences between S100A1 and other S100 proteins (*i.e.* S100B) that are necessary to understand its specific biological functions (Cavalier, Ansari *et al.*, 2016; Donato *et al.*, 2013; Lin *et al.*, 2010; Wright, Prosser *et al.*, 2008; Zimmer *et al.*, 1995). These data can be used to aid in the development of more specific, efficacious inhibitors that target one S100 protein *versus* another. They also provide support for the modeling of the Ca^{2+} ion coordination sphere by previous NMR studies, which is necessary to understand the role that S100A1 plays as a calcium-signaling protein in mammals. While numerous similarities are found among S100-family members, including their global fold and overall Ca^{2+}-dependent conformational change, detailed differences need to be catalogued in order to understand their specific S100–target protein interactions and perhaps for the development of therapeutics targeting such family members in various disease states. Some of these differences include one of the Ca^{2+}-coordinating residues (Asn65 in S100A1 and Asp65 in S100B), numerous residues in the binding pocket of the two proteins (Figs. 2 and 3), and other residues throughout the protein that are likely to affect the binding and functional folding events associated with increasing Ca^{2+} binding upon binding its specific protein targets. The crystal structure of Ca^{2+}-S100A1 will also have an impact on our understanding of protein–protein interactions involving S100A1 with full-length targets such as the ryanodine receptors in skeletal (RyR1) and cardiac (RyR2) muscle as well as how it responds to Ca^{2+} concentration fluctuations within mammalian cells (Hernández-Ochoa *et al.*, 2009; Prosser *et al.*, 2008, 2011; Wright, Prosser *et al.*, 2008).

Acknowledgements

Use of the Stanford Synchrotron Radiation Lightsource, SLAC National Accelerator Laboratory is supported by the US DOE, Office of Science and Office of Basic Energy. The SSRL Structural Molecular Biology Program is supported by the DOE Office of Biological and Environmental Research and by the National Institutes of Health, National Institute of General Medical Sciences. This work was also supported by NIH grants (CA107331 and GM58888 to DJW). The training of ZM was also supported by an NIH grant (NIH T32 AR007592). We also thank Drs Michael C. Cavalier and Sean D. Stowe for advice with solving this crystal structure.

References

Adams, P. D. *et al.* (2010). *Acta Cryst.* D**66**, 213–221.
Afonine, P. V., Grosse-Kunstleve, R. W., Echols, N., Headd, J. J., Moriarty, N. W., Mustyakimov, M., Terwilliger, T. C., Urzhumtsev, A., Zwart, P. H. & Adams, P. D. (2012). *Acta Cryst.* D**68**, 352–367.
Baudier, J., Glasser, N. & Gerard, D. (1986). *J. Biol. Chem.* **261**, 8192–8203.
Bresnick, A. R., Weber, D. J. & Zimmer, D. B. (2015). *Nature Rev. Cancer*, **15**, 96–109.
Bricogne, G., Blanc, E., Brandl, M., Flensburg, C., Keller, P., Paciorek, W., Roversi, P., Sharff, A., Smart, O. S., Vonrhein, C. & Womack, T. O. (2016). *BUSTER*. Cambridge: Global Phasing Ltd.
Cavalier, M. C., Ansari, M. I., Pierce, A. D., Wilder, P. T., McKnight, L. E., Raman, E. P., Neau, D. B., Bezawada, P., Alasady, M. J., Charpentier, T. H., Varney, K. M., Toth, E. A., MacKerell, A. D., Coop, A. & Weber, D. J. (2016). *J. Med. Chem.* **59**, 592–608.
Cavalier, M. C., Melville, Z., Aligholizadeh, E., Raman, E. P., Yu, W., Fang, L., Alasady, M., Pierce, A. D., Wilder, P. T., MacKerell, A. D. & Weber, D. J. (2016). *Acta Cryst.* D**72**, 753–760.
Cavalier, M. C., Pierce, A. D., Wilder, P. T., Alasady, M. J., Hartman, K. G., Neau, D. B., Foley, T. L., Jadhav, A., Maloney, D. J., Simeonov, A., Toth, E. A. & Weber, D. J. (2014). *Biochemistry*, **53**, 6628–6640.
Charpentier, T. H., Thompson, L. E., Liriano, M. A., Varney, K. M., Wilder, P. T., Pozharski, E., Toth, E. A. & Weber, D. J. (2010). *J. Mol. Biol.* **396**, 1227–1243.
Charpentier, T. H., Wilder, P. T., Liriano, M. A., Varney, K. M., Zhong, S., Coop, A., Pozharski, E., MacKerell, A. D., Toth, E. A. & Weber, D. J. (2009). *Biochemistry*, **48**, 6202–6212.
Cohen, A. E., Ellis, P. J., Miller, M. D., Deacon, A. M. & Phizackerley, R. P. (2002). *J. Appl. Cryst.* **35**, 720–726.
Czodrowski, P., Dramburg, I., Sotriffer, C. A. & Klebe, G. (2006). *Proteins*, **65**, 424–437.
Di Tommaso, P., Moretti, S., Xenarios, I., Orobitg, M., Montanyola, A., Chang, J.-M., Taly, J.-F. & Notredame, C. (2011). *Nucleic Acids Res.* **39**, W13–W17.
Dolinsky, T. J., Czodrowski, P., Li, H., Nielsen, J. E., Jensen, J. H., Klebe, G. & Baker, N. A. (2007). *Nucleic Acids Res.* **35**, W522–W525.
Dolinsky, T. J., Nielsen, J. E., McCammon, J. A. & Baker, N. A. (2004). *Nucleic Acids Res.* **32**, W665–W667.
Donato, R. (2001). *Int. J. Biochem. Cell Biol.* **33**, 637–668.
Donato, R., Cannon, B. R., Sorci, G., Riuzzi, F., Hsu, K., Weber, D. J. & Geczy, C. L. (2013). *Curr. Mol. Med.* **13**, 24–57.
Drohat, A. C., Baldisseri, D. M., Rustandi, R. R. & Weber, D. J. (1998). *Biochemistry*, **37**, 2729–2740.
Emsley, P., Lohkamp, B., Scott, W. G. & Cowtan, K. (2010). *Acta Cryst.* D**66**, 486–501.
Garbuglia, M., Verzini, M., Rustandi, R. R., Osterloh, D., Weber, D. J., Gerke, V. & Donato, R. (1999). *Biochem. Biophys. Res. Commun.* **254**, 36–41.
Gógl, G., Alexa, A., Kiss, B., Katona, G., Kovács, M., Bodor, A., Reményi, A. & Nyitray, L. (2016). *J. Biol. Chem.* **291**, 11–27.
González, A., Moorhead, P., McPhillips, S. E., Song, J., Sharp, K., Taylor, J. R., Adams, P. D., Sauter, N. K. & Soltis, S. M. (2008). *J. Appl. Cryst.* **41**, 176–184.
González, A. & Tsai, Y. A. (2010). *A Quick XDS Tutorial for SSRL*. http://smb.slac.stanford.edu/facilities/software/xds/#autoxds_script.
Harpio, R. & Einarsson, R. (2004). *Clin. Biochem.* **37**, 512–518.
Hernández-Ochoa, E. O., Prosser, B. L., Wright, N. T., Contreras, M., Weber, D. J. & Schneider, M. F. (2009). *Am. J. Physiol. Cell Physiol.* **297**, C955–C970.
Jensen, J. L., Indurthi, V. S. K., Neau, D. B., Vetter, S. W. & Colbert, C. L. (2015). *Acta Cryst.* D**71**, 1176–1183.
Kabsch, W. (2010). *Acta Cryst.* D**66**, 125–132.
Kligman, D. & Hilt, D. C. (1988). *Trends Biochem. Sci.* **13**, 437–443.
Landar, A., Rustandi, R. R., Weber, D. J. & Zimmer, D. B. (1998). *Biochemistry*, **37**, 17429–17438.
Lebedev, A. A. & Isupov, M. N. (2014). *Acta Cryst.* D**70**, 2430–2443.

Lin, J., Yang, Q., Wilder, P. T., Carrier, F. & Weber, D. J. (2010). *J. Biol. Chem.* **285**, 27487–27498.
Liriano, M. A., Varney, K. M., Wright, N. T., Hoffman, C. L., Toth, E. A., Ishima, R. & Weber, D. J. (2012). *J. Mol. Biol.* **423**, 365–385.
Long, F., Vagin, A. A., Young, P. & Murshudov, G. N. (2008). *Acta Cryst.* D**64**, 125–132.
Malashkevich, V. N., Varney, K. M., Garrett, S. C., Wilder, P. T., Knight, D., Charpentier, T. H., Ramagopal, U. A., Almo, S. C., Weber, D. J. & Bresnick, A. R. (2008). *Biochemistry*, **47**, 5111–5126.
Matsumura, H., Shiba, T., Inoue, T., Harada, S. & Kai, Y. (1998). *Structure*, **6**, 233–241.
Moroz, O. V., Bronstein, I. B. & Wilson, K. S. (2011). *J. Mol. Biol.* **411**, 1072–1082.
Most, P., Pleger, S. T., Völkers, M., Heidt, B., Boerries, M., Weichenhan, D., Löffler, E., Janssen, P. M. L., Eckhart, A. D., Martini, J., Williams, M. L., Katus, H. A., Remppis, A. & Koch, W. J. (2004). *J. Clin. Invest.* **114**, 1550–1563.
Most, P., Remppis, A., Pleger, S. T., Katus, H. A. & Koch, W. J. (2007). *Am. J. Physiol. Regul. Integr. Comput. Physiol.* **293**, R568–R577.
Most, P., Remppis, A., Pleger, S. T. *et al.* (2003). *J. Biol. Chem.* **278**, 33809–33817.
Most, P., Remppis, A., Weber, C., Bernotat, J., Ehlermann, P., Pleger, S. T., Kirsch, W., Weber, M., Uttenweiler, D., Smith, G. L., Katus, H. A. & Fink, R. H. A. (2003). *J. Biol. Chem.* **278**, 26356–26364.
Notredame, C., Higgins, D. G. & Heringa, J. (2000). *J. Mol. Biol.* **302**, 205–217.
Nowakowski, M., Ruszczyńska-Bartnik, K., Budzińska, M., Jaremko, Ł., Jaremko, M., Zdanowski, K., Bierzyński, A. & Ejchart, A. (2013). *Biochemistry*, **52**, 1149–1159.
Osterloh, D., Ivanenkov, V. V. & Gerke, V. (1998). *Cell Calcium*, **24**, 137–151.
Pettersen, E. F., Goddard, T. D., Huang, C. C., Couch, G. S., Greenblatt, D. M., Meng, E. C. & Ferrin, T. E. (2004). *J. Comput. Chem.* **25**, 1605–1612.
Prosser, B. L., Hernández-Ochoa, E. O. & Schneider, M. F. (2011). *Cell Calcium*, **50**, 323–331.
Prosser, B. L., Wright, N. T., Hernãndez-Ochoa, E. O., Varney, K. M., Liu, Y., Olojo, R. O., Zimmer, D. B., Weber, D. J. & Schneider, M. F. (2008). *J. Biol. Chem.* **283**, 5046–5057.
Rustandi, R. R., Drohat, A. C., Baldisseri, D. M., Wilder, P. T. & Weber, D. J. (1998). *Biochemistry*, **37**, 1951–1960.
Salama, I., Malone, P. S., Mihaimeed, F. & Jones, J. L. (2008). *Eur. J. Surg. Oncol.* **34**, 357–364.
Schäfer, B. W. & Heizmann, C. W. (1996). *Trends Biochem. Sci.* **21**, 134–140.
Schneider, M. C., Prosser, B. E., Caesar, J. J. E., Kugelberg, E., Li, S., Zhang, Q., Quoraishi, S., Lovett, J. E., Deane, J. E., Sim, R. B., Roversi, P., Johnson, S., Tang, C. M. & Lea, S. M. (2009). *Nature (London)*, **458**, 890–893.
Soltis, S. M. *et al.* (2008). *Acta Cryst.* D**64**, 1210–1221.
Strynadka, N. C. J. & James, M. N. G. (1989). *Annu. Rev. Biochem.* **58**, 951–999.
Treves, S., Scutari, E., Robert, M., Groh, S., Ottolia, M., Prestipino, G., Ronjat, M. & Zorzato, F. (1997). *Biochemistry*, **36**, 11496–11503.
Vagin, A. A. (1989). *Jnt CCP4–ESF–EACBM Newsl. Protein Crystallogr.* **24**, 117–121.
Vagin, A. & Teplyakov, A. (1997). *J. Appl. Cryst.* **30**, 1022–1025.
Vagin, A. & Teplyakov, A. (2010). *Acta Cryst.* D**66**, 22–25.
Wang, G., Zhang, S., Fernig, D. G., Martin-Fernandez, M., Rudland, P. S. & Barraclough, R. (2005). *Oncogene*, **24**, 1445–1454.
Wilder, P. T., Baldisseri, D. M., Udan, R., Vallely, K. M. & Weber, D. J. (2003). *Biochemistry*, **42**, 13410–13421.
Wright, N. T., Cannon, B. R., Wilder, P. T., Morgan, M. T., Varney, K. M., Zimmer, D. B. & Weber, D. J. (2009). *J. Mol. Biol.* **386**, 1265–1277.
Wright, N. T., Inman, K. G., Levine, J. A., Cannon, B. R., Varney, K. M. & Weber, D. J. (2008). *J. Biomol. NMR*, **42**, 279–286.
Wright, N. T., Prosser, B. L., Varney, K. M., Zimmer, D. B., Schneider, M. F. & Weber, D. J. (2008). *J. Biol. Chem.* **283**, 26676–26683.
Wright, N. T., Varney, K. M., Ellis, K. C., Markowitz, J., Gitti, R. K., Zimmer, D. B. & Weber, D. J. (2005). *J. Mol. Biol.* **353**, 410–426.
Yamaguchi, N., Prosser, B. L., Ghassemi, F., Xu, L., Pasek, D. A., Eu, J. P., Hernández-Ochoa, E. O., Cannon, B. R., Wilder, P. T., Lovering, R. M., Weber, D., Melzer, W., Schneider, M. F. & Meissner, G. (2011). *Am. J. Physiol. Cell Physiol.* **300**, C998–C1012.
Zimmer, D. B., Cornwall, E. H., Landar, A. & Song, W. (1995). *Brain Res. Bull.* **37**, 417–429.
Zimmer, D. B., Cornwall, E. H., Reynolds, P. D. & Donald, C. M. (1998). *J. Biol. Chem.* **273**, 4705–4711.
Zimmer, D. B. & Weber, D. J. (2010). *Cardiovasc. Psychiatr. Neurol.*, **2010**, 728052.